ACS APPLIED NANO MATERIALS

www.acsanm.org Article

Ligand Substitution of UiO-66-2OH for Universal Phosphate Detection

Jiansen Wang, Yihong Zhang, Yuting Wang, Qi Sun, and Hui Wei*

Cite This: *ACS Appl. Nano Mater.* 2024, 7, 19466−19472 Read Online

ACCESS | Metrics & More | Article Recommendations | Supporting Information

ABSTRACT: Phosphate plays a crucial role in biological metabolism across both plants and animals, with abnormal concentrations often indicating various diseases. Despite the prevalence of the molybdenum blue detection method, certain issues persist, including difficulties in preservation and the need for fresh preparation. Here, we introduce a hydroxy-modified metal−organic framework, University of Oslo 66 (UiO-66-2OH), as a versatile platform for fluorescence probes capable of detecting phosphate concentrations in both botanical and clinical contexts. By changing modulator amounts and metal centers, we synthesized particles of varying sizes and active centers (Zr and Hf). Our investigations revealed that a 300 nm UiO-66-2OH particle with a Zr center was optimal for phosphate detection, achieving a limit of detection of 7 μM with low cost. Furthermore, we explored the potential agricultural and diagnostic applications. These findings underscored the versatility and promise of UiO-66-2OH as a sensing material for diverse biological and medical applications.

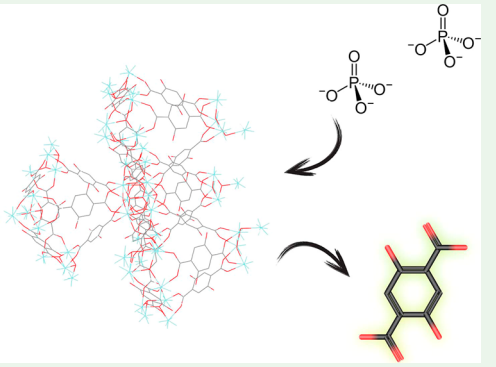

KEYWORDS: *fluorescence, phosphate, metal−organic framework, chronic kidney disease, barley phosphate insufficiency*

INTRODUCTION

Phosphate plays a critical role in many biological processes such as energy metabolism[1,2] and cellular signaling.[3] Insufficient phosphate concentration in the culture medium can inhibit the phosphate absorption in plants, thus inhibiting plant growth and development.[4,5] In humans, abnormal phosphate concentration indicates potential diseases.[6,7] For example, hyperphosphatemia could indicate chronic kidney disease, in which phosphate could not be easily filtered by the kidney and would accumulate in the serum.[8]

One of the most prevalent detection methods of phosphate concentration involves the reaction between phosphate ions and ammonium molybdate since it was first developed in 1969.[9] Phosphomolybdic acid is reduced to molybdenum blue (MoB), which has a characteristic absorbance at 650 nm. Some researchers have developed microfluid sensors based on this method[10] and even combined this with a smart phone.[11] However, due to the nature of ammonium molybdate redox reaction, this process involves toxic dichloroacetic acid to remove protein and the solution cannot be preserved for long.[12] Some other methods have also been developed to detect organic and inorganic phosphate compounds. Most methods were under the principle that phosphate could induce the fluorescence emission of certain materials, such as luminescent lanthanide-functionalized coordination polymer[13] or fluorophore bound to a bacterial phosphate-binding protein.[14] Some of these methods use materials that could be broken down by phosphate and thus release the probe, such as Rhodamine B (RhB),[15] while others made use of materials with active sites that could be blocked/activated by phosphates.[16−18] Some other methods, such as ion-selective electrodes, were also developed.[19] Nevertheless, they were not commercialized for some reasons such as accuracy, cost performance, or potential pollution.

Metal−organic frameworks (MOFs) are a class of materials comprised of metal ions or clusters coordinated with organic ligands to form porous structures. Researchers from the University of Oslo in Norway first synthesized UiO-66 in 2008.[20] The development of the crystal could be described as the process of metal oxide centers linked together by linkers.[21] By preclustering metal oxide centers, we could link fluorescent linkers with high steric hindrance onto the Lewis acid. This process could be slowed down by modulators, such as acetic acid, to form octahedron crystals during synthesis. The metal center made it a potential candidate for ion detection due to the interaction between metal ions and linkers.[22] By controlling the modulator's amount, we could synthesize different sizes of materials to control the speed of the detecting reaction.

Received: June 12, 2024
Revised: July 30, 2024
Accepted: July 31, 2024
Published: August 13, 2024

https://doi.org/10.1021/acsanm.4c03379
ACS Appl. Nano Mater. 2024, 7, 19466−19472

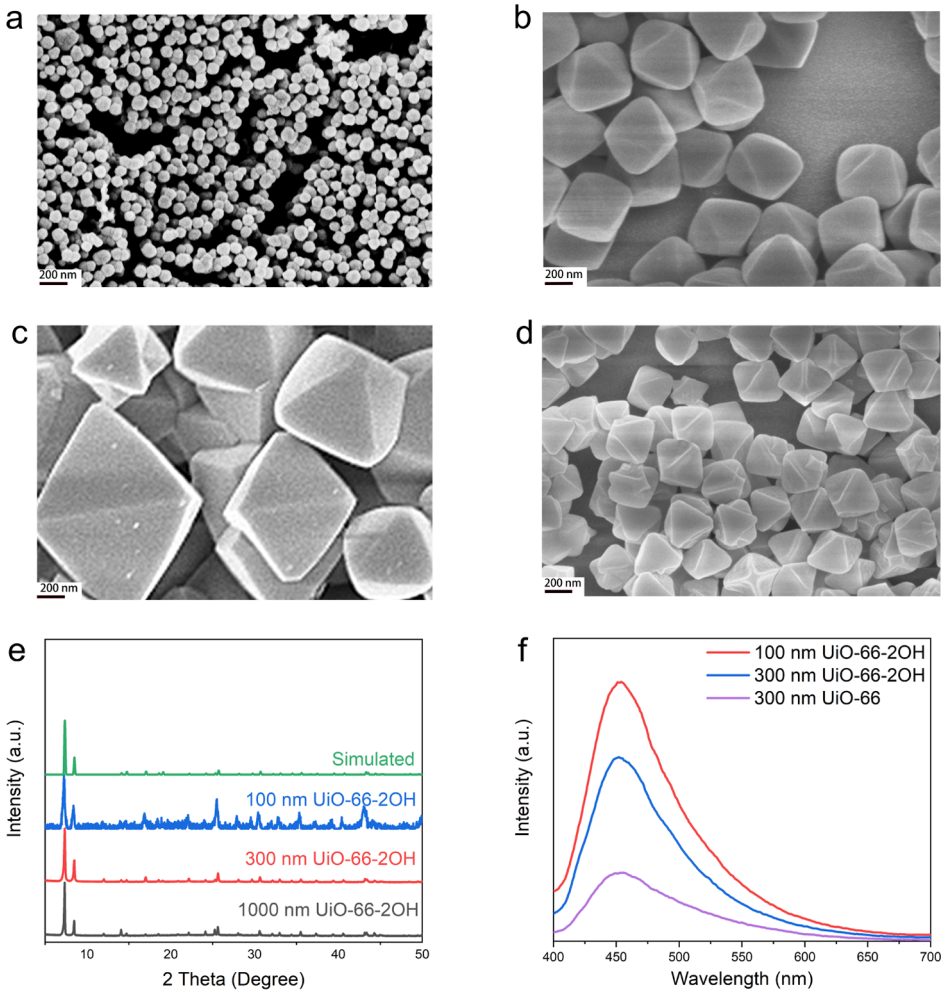

Figure 1. SEM images of (a) 100, (b) 300, and (c) 1000 nm UiO-66-2OH and (d) 300 nm Hf-centered UiO-66-2OH. (e) XRD patterns of as-synthesized UiO-66-2OH. (f) Fluorescence intensity of different sizes of 0.1 mg/mL UiO-66-2OH and UiO-66. λ_{ex} = 365 nm.

Here, we aimed to develop a sensitive and specific phosphate detection probe. We synthesized a series of UiO-66 MOFs based on the interaction between the Lewis acid center and phosphate. Then, we optimized the sensitivity by changing the metal center and optimized reaction speed by modulating particle size. Importantly, phosphate concentrations in two different models: a barley phosphate deficiency model and a chronic kidney disease model were successfully detected.

RESULTS AND DISCUSSION

Synthesis and Characterizations of UiO-66-2OH. We prepared UiO-66-2OH through a hydrothermal process using acetic acid as a size modulator. We chose 2,5-dihydroxyterephthalic acid (BDC-2OH) as the linker because it has a typical fluorescence pattern. We also changed the metal salt with different Lewis acidities to obtain UiO-66-2OH with different metal centers [(Hf)UiO-66-2OH and (Zr)UiO-66-2OH] in order to reach the desired interaction between UiO-66-2OH and phosphate. UiO-66-2OH referred to Zr-centered particles unless otherwise mentioned. As shown in Figure 1a–d, the scanning electron microscope (SEM) images revealed that the size of UiO-66-2OH nanoparticles was uniform. The 300 and 1000 nm samples had a classic regular octahedron shape. However, as shown in Figure S3, the 1000 nm sample would precipitate in water with time, so we did not do any further tests using the 1000 nm sample. Compared with UiO-66 in Figures S1 and S4, the edges of UiO-66-2OH were dull, indicating that UiO-66-2OH has weaker crystallinity than UiO-66. We could attribute this phenomenon to the change of the molar ratio between the ligand and metal center.[23] The X-ray diffraction (XRD) patterns in Figure 1e of the as-synthesized UiO-66-2OH had two major peaks separately at 7.3 and 8.5°, which was in accordance with that of the simulated pattern, indicating that the UiO-66-2OH was well-synthesized.

As shown in Figure 1f, the emission peak of UiO-66-2OH was in accordance with that of UiO-66. This indicated that the structure of the MOF caused the emission peak at 450 nm. The fluorescence intensity was size-dependent, indicating that the outer layer of the linker gave out the fluorescence peak. This was because the small-sized UiO-66-2OH had more outer surface than the larger one under the same mass conditions. The intensity of UiO-66 was weaker than that of UiO-66-2OH with the same size, indicating that the defect on the surface gave out the fluorescence peak. This was because the crystallinity of UiO-66 (Figure S1) was better than that of UiO-66-2OH. The peak of UiO-66-2OH was away from that of BDC-2OH, which ensured that the fluorescence of UiO-66-2OH would not interfere with that of BDC-2OH.

https://doi.org/10.1021/acsanm.4c03379
ACS Appl. Nano Mater. 2024, 7, 19466−19472

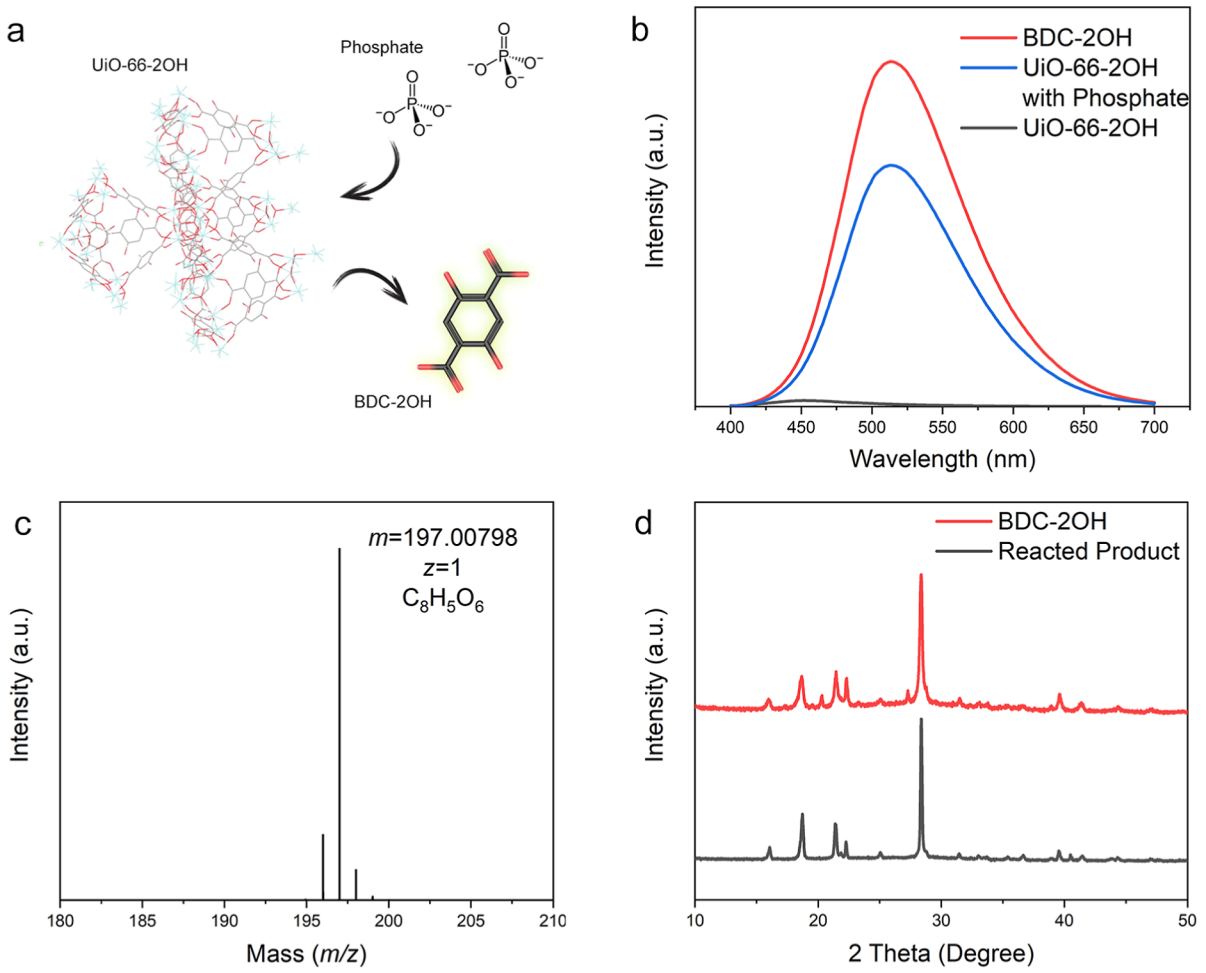

Figure 2. (a) Illustration of phosphate-induced breakdown of zirconium-centered UiO-66-2OH. (b) Fluorescence intensity of pure UiO-66-2OH, UiO-66-2OH with phosphate, and BDC-2OH. λ_{ex} = 365 nm. (c) Mass spectrum of the degraded product. (d) XRD patterns of pure BDC-2OH and the reacted product.

Phosphate-Induced Breakdown of UiO-66-2OH. Phosphate could interact with strong Lewis acids such as transition metals.[24] The phosphate ions could substitute the organic linker bond on the metal center and release the linker into the solution (Figure 2a). As shown in Figure 2b, under the excitation of 365 nm ultraviolet light, the sample produced a strong luminescence at 540 nm, which was in accordance with that of the chosen linker, while the synthesized UiO-66-2OH particles only have a minor emission peak at 450 nm. We then studied the composition of the reacted solution by mass spectroscopy and XRD. The mass spectrum of the supernatant in Figure 2c also indicated that the supernatant mostly contained BDC-2OH. HCl was introduced to the reacted solution to achieve precipitation. As shown in Figure 2d, the diffraction pattern was in accordance with that of pure BDC-2OH. We could conclude that the released BDC-2OH would not interact with other compositions in the solution, meaning that the fluorescence was given by the released BDC-2OH when phosphate was added into the solution.

After all the phosphate bonded at the metal center, the fluorescence intensity at 540 nm stayed constant with time. To obtain a suitable reaction rate, we compared between different sizes of UiO-66-2OH. As we could see in Figure S5, the rate of the reaction decreased with the particle size, together with the SEM images before and after the reaction (Figures 1b and S2), indicating that the reaction happened at the surface of the particle, thus indicating that we could decrease the particle size to shorten the reaction time. Meanwhile, during the batch synthesis, conventional methods were poor in mass/thermal transfer,[25] which would cause a wider distribution of particle size. In Figure S5, the end point was not relevant to the particle size; both the large and small particles did not affect the accuracy of the detection. This indicates that the reaction can be scaled up to an industrial production without compromising the precision of this detection method.

To find out if pH could affect the coordination ability between phosphate and metal oxide clusters owing to the coordination competition between Zr−O and H−O, we further tested whether the pH would change during the reaction and cause error. As shown in Figure S6, we adjusted the pH of three groups of solutions to around 7.4 using HCl and NaOH. After adding 10% volume 1 mg/mL UiO-66-2OH, the pH dropped to around 7 and stayed the same after the reaction, which indicated that the OH^--capturing ability of Zr−O clusters could stabilize the pH of the reaction.

Selectivity of Serum-Containing Substances. To find out if the substances in the serum other than phosphate had influence on the test results, we mapped out the possible substances that occur in the serum using a microplate reader. As shown in Figure 3a, in the simulated solution, only

https://doi.org/10.1021/acsanm.4c03379
ACS Appl. Nano Mater. 2024, 7, 19466−19472

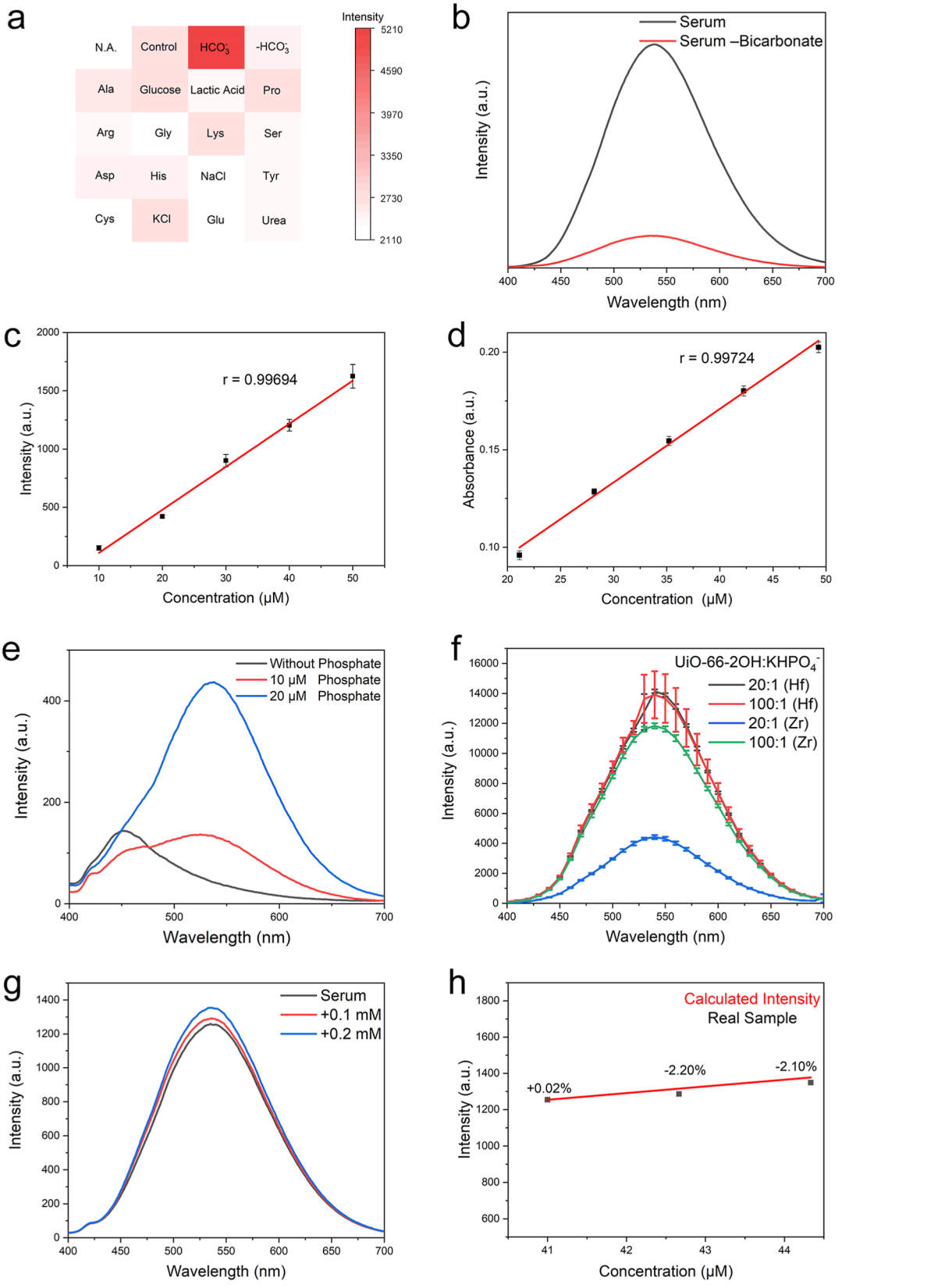

Figure 3. (a) Fluorescence intensity with potentially interfering substances together with phosphate. (b) Fluorescence with pure serum and bicarbonate-removed serum. λ_{ex} = 365 nm. (c) Fluorescence intensity of UiO-66-2OH versus serum adding different amounts of phosphate. λ_{ex} = 365 nm. (d) Fluorescence intensity of UiO-66-2OH versus calculated phosphate concentration. λ_{ex} = 365 nm. (e) Fitting plot of fluorescence intensity of UiO-66-2OH versus phosphate concentration. λ_{ex} = 365 nm. (f) Fitting plot of absorbance of MoB versus phosphate concentration. λ_{ex} = 365 nm. (g) Fluorescence intensity under low phosphate concentration. λ_{ex} = 365 nm. (h) Fluorescence intensity under overdose phosphate concentration. λ_{ex} = 365 nm.

https://doi.org/10.1021/acsanm.4c03379
ACS Appl. Nano Mater. 2024, 7, 19466−19472

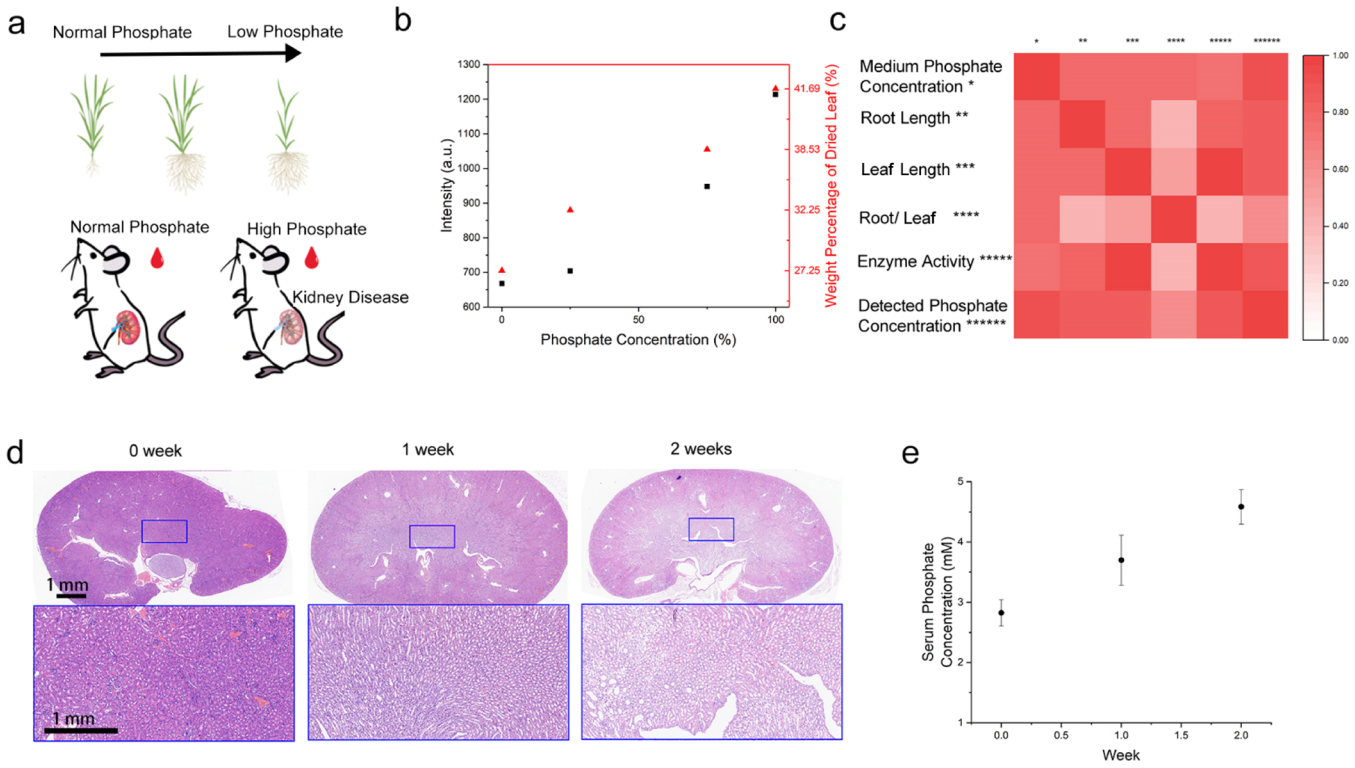

Figure 4. (a) Illustration of two detection methods. (b) Detected fluorescent intensity of samples and weight percentage of dried leaves cultivated in media containing different phosphate concentrations. λ_{ex} = 365 nm. (c) Correlation between medium phosphate concentration, root length, leaf length, root length/leaf length, enzyme activity, and detected phosphate concentration. (d) H&E-stained samples of BALB/c mouse kidney after 0, 1, and 2 weeks of adenine oral gavage. (e) Detected serum phosphate concentration via this method.

bicarbonate ions had a considerable effect on the final fluorescence intensity. We removed the bicarbonate by simply excluding it with HCl. After removing bicarbonate using 1 M HCl, tuning pH to 7.4 with NaOH and centrifuging to remove the excess amount of UiO-66-2OH, the fluorescence intensity returned to a normal range. As shown in Figure 3b, bicarbonate had an influence on the serum sample. This also indicated that our method was capable of bicarbonate detection by calculating the intensity gap before and after adding HCl. We did not consider the potential effect of protein in the serum because the protein would be salted out by excessive amounts of HCl and NaOH and centrifuged together with excess UiO-66-2OH. This was also confirmed by the further comparison between standard MoB colorimetry and this method. The detection results without removing protein were the same as the standard method.

Comparison with Traditional MoB Colorimetry. We chose the standard MoB method for comparison. We separately standardized two methods. The phosphate concentration range of the MoB (Figure 3c) method was narrower than that of our method (Figure 3d). This was because the Beer–Lambert law was only applicable when the absorbance was around 0.5 and could not be applied to a too diluted or concentrated solution. The correlation between fluorescence intensity (I) and phosphate concentration (c) was $I = 36.93 \times c - 259.91$. The constant part of this equation reflected the coordination ability of the metal center and phosphate. The Pearson's correlation coefficients of both methods were in the same range. The limit of detection (LOD) of phosphate by UiO-66-2OH was calculated to be 7.03 μM. As shown in Figure 3e, the 10 μM sample could be vividly distinguished from the blank sample. Adjusting the UiO-66-2OH concentration could affect the LOD. This was because when the concentration of phosphate was too low compared with UiO-66-2OH, the phosphate would be linked on the defection instead of breaking the MOF structure. As shown in Figure 3f, an experiment with a high UiO-66-2OH concentration confirmed this. The fluorescence intensity with higher amounts of UiO-66-2OH was reduced. We further synthesized Hf-centered UiO-66-2OH to confirm if the cause was coordination ability (Figure S4). As we could see in Figure 3f, no obvious change occurred when (Hf)UiO-66-2OH/HPO_4^- increased from 20:1 to 100:1. This also indicated that the LOD of (Hf)UiO-66-2OH would be much higher than that of (Zr)UiO-66-2OH. But it was worth noticing that the cost of the Hf probe was way higher than that of Zr.

Detection of Phosphate Concentration in Bovine Serum. We tested our method in purchased bovine serum. We determined the phosphate concentration of purchased bovine serum to be 2.46 mM using the standard MoB method, which was in the normal range of bovine.[26] We prepared two other samples by adding K_2HPO_4 and the phosphate concentration was adjusted to 2.56 and 2.66 mM, respectively. The obtained serum sample was diluted 60 times and the bicarbonate was removed using HCl. After adjusting the pH back to 7.4, we added UiO-66-2OH and reacted it for 1 h at 37 °C. As shown in Figure 3g, the fluorescence intensity at 540 nm of the obtained and centrifuged samples was 1255, 1289, and 1349, respectively, and the calculated concentration was 2.46, 2.52, and 2.61 mM, which was 100, 98, and 98% in accordance with the concentration given by the MoB method (Figure 3h). This also strongly suggested that nothing in the serum other than phosphate had influence on the breakdown of UiO-66-2OH.

https://doi.org/10.1021/acsanm.4c03379
ACS Appl. Nano Mater. 2024, 7, 19466–19472

Detection of Phosphate Concentration in Barley. For agriculture, there exists a series of trade-offs between root system morphology, mycorrhizal symbiosis, and root exudation to optimize phosphate acquisition under limited phosphate conditions (Figure 4a). A lack of phosphate would cause poor root development, reduced photosynthesis, and eventually overall reduced growth.[27] Therefore, in order to overcome phosphate limitations in soil and increase crop yield, large amounts of phosphate fertilizers were used worldwide. However, microbial activity would either adsorb or oxidize excess amounts of phosphate fertilizers. Excessive use of phosphate fertilizers can lead to environmental pollution, such as eutrophication, and waste of natural phosphate resources. Phosphate concentration should be measured to fertilize precisely. We successfully detected the phosphate concentration. Using this method, the detected phosphate concentration could be used to predict growth deficiency. To test out the robustness of this method on agricultural use, we cultivated a set of barley plants by using a hydroponics system with different phosphate concentrations of 50, 100, 150, and 200 μM (25, 50, 75, and 100%). After 10 days of cultivation, we divided and sampled the barley plants individually using ImageJ. As shown in Figures 4b and S7, the barley leaves cultivated in the high phosphate-containing medium were longer than those cultivated in a medium of low phosphate concentration. As some previous studies had revealed, we could attribute this to phosphate acquisition.[27] As shown in Figures 4c and S7, the different growth factors such as root length, leaf length, and alkaline phosphatase in root area showed great correlation with the phosphate concentration in barley plants and culturing medium using this method. By monitoring phosphate concentration in both the plant and the culturing medium, we could approach precise fertilization.

Detection for Serum Phosphate in the Chronic Kidney Disease Model. We also tested our method using the chronic kidney disease model (Figure 4a). Phosphate levels were primarily regulated by the kidney.[28] Through serum phosphate detection, we could reveal kidney dysfunction. To test out the potential of this method in clinical situations, we established the chronic kidney disease model in mice. After 2 weeks of adenine oral gavage, we successfully established the chronic kidney disease model in BALB/c mice.

Samples were randomly chosen for serum phosphate detection at the end of each week. As we could see in Figure 4d, after 2 weeks of adenine gavage, the renal medulla expanded drastically and the kidney lost most of its filtering ability, thus increasing serum phosphate concentration (Figure 4e). Using our method, the observed serum phosphate concentrations accurately reflected the kidney damage process.

CONCLUSIONS

Phosphate plays a critical role in many biological processes. Monitoring phosphate concentration can contribute to agriculture and clinical detection. However, traditional detection methods were not sensitive enough and had economic concerns. In this work, we synthesized different sizes of UiO-66-2OH to detect serum phosphate with high efficiency, storage stability, and low cost (Table S1). Based on the coordination competition reaction between active center/phosphate and active center/linker, this detection method could reach a LOD of 7 μM, and the LOD could be lowered by changing the metal center. UiO-66-2OH was quite stable due to its high tolerance toward partial lattice collapse.[20,29] After studying the budget, the Zr-centered probe cost less than 0.5 $ every 1000 times. To confirm our method as a universal approach to detect phosphate concentration, we tested our method in several real-life scenarios. We established a phosphate deficiency model on barley and a chronic kidney disease model on mice. We successfully detected phosphate deficiency using barley leaves as the sample and predicted kidney disease using serum as the sample. These results suggested that this method was sufficient for phosphate measurement.

ASSOCIATED CONTENT

Supporting Information

The Supporting Information is available free of charge at https://pubs.acs.org/doi/10.1021/acsanm.4c03379.

Experimental details; figures including SEM and digital images of the referred content, XRD patterns, pH environment of reaction, and fluorescent comparison between different samples; and table for comparison of different detection methods (PDF)

AUTHOR INFORMATION

Corresponding Author

Hui Wei − *College of Engineering and Applied Sciences, Nanjing National Laboratory of Microstructures, Jiangsu Key Laboratory of Artificial Functional Materials, Nanjing University, Nanjing, Jiangsu 210023, China; State Key Laboratory of Analytical Chemistry for Life Science, School of Chemistry and Chemical Engineering, Chemistry and Biomedicine Innovation Center (ChemBIC), Nanjing University, Nanjing, Jiangsu 210023, China;* orcid.org/0000-0003-0870-7142; Email: weihui@nju.edu.cn

Authors

Jiansen Wang − *College of Engineering and Applied Sciences, Nanjing National Laboratory of Microstructures, Jiangsu Key Laboratory of Artificial Functional Materials, Nanjing University, Nanjing, Jiangsu 210023, China*

Yihong Zhang − *College of Engineering and Applied Sciences, Nanjing National Laboratory of Microstructures, Jiangsu Key Laboratory of Artificial Functional Materials, Nanjing University, Nanjing, Jiangsu 210023, China*

Yuting Wang − *College of Engineering and Applied Sciences, Nanjing National Laboratory of Microstructures, Jiangsu Key Laboratory of Artificial Functional Materials, Nanjing University, Nanjing, Jiangsu 210023, China*

Qi Sun − *School of Chemistry and Chemical Engineering, Nanjing University, Nanjing, Jiangsu 210023, China*

Complete contact information is available at: https://pubs.acs.org/10.1021/acsanm.4c03379

Funding

This work was funded by the National Natural Science Foundation of China (22374071), the National Key R&D Program of China (2021YFF1200700 and 2019YFA0709200), Jiangsu Provincial Key R&D Program (BE2022836), the PAPD Program, State Key Laboratory of Analytical Chemistry for Life Science (5431ZZXM2306), NMPA Key Laboratory for Biomedical Optics (20240001), and Fundamental Research Funds for the Central Universities (202200325, 021314380228, and 021314380195).

Notes

The authors declare no competing financial interest.

■ ACKNOWLEDGMENTS

We thank Dr. Yufei Jiang for performing mass spectroscopy.

■ REFERENCES

(1) Beyer, K.; Klingenberg, M. ADP/ATP carrier protein from beef heart mitochondria has high amounts of tightly bound cardiolipin, as revealed by phosphorus-31 nuclear magnetic resonance. *Biochemistry* **1985**, *24*, 3821−3826.
(2) Duff, S. M. G.; Sarath, G.; Plaxton, W. C. The role of acid phosphatases in plant phosphorus metabolism. *Physiol. Plant.* **1994**, *90*, 791−800.
(3) Michell, B. Early steps along the road to inositol-lipid-based signalling. *Trends Biochem. Sci.* **1995**, *20*, 326−329.
(4) Shen, J.; Yuan, L.; Zhang, J.; Li, H.; Bai, Z.; Chen, X.; Zhang, W.; Zhang, F. Phosphorus Dynamics: From Soil to Plant. *Plant Physiol.* **2011**, *156*, 997−1005.
(5) Schachtman, D. P.; Reid, R. J.; Ayling, S. M. Phosphorus Uptake by Plants: From Soil to Cell. *Plant Physiol.* **1998**, *116*, 447−453.
(6) Florenzano, P.; Cipriani, C.; Roszko, K. L.; Fukumoto, S.; Collins, M. T.; Minisola, S.; Pepe, J. Approach to patients with hypophosphataemia. *Lancet Diabetes Endocrinol.* **2020**, *8*, 163−174.
(7) Weisinger, J. R.; Bellorín-Font, E. Magnesium and phosphorus. *Lancet* **1998**, *352*, 391−396.
(8) Levey, A. S.; Coresh, J. Chronic kidney disease. *Lancet* **2012**, *379*, 165−180.
(9) Eibl, H.; Lands, W. E. M. A new, sensitive determination of phosphate. *Anal. Biochem.* **1969**, *30*, 51−57.
(10) McGraw, C. M.; Stitzel, S. E.; Cleary, J.; Slater, C.; Diamond, D. Autonomous microfluidic system for phosphate detection. *Talanta* **2007**, *71*, 1180−1185.
(11) Ray, A.; Esparza, S.; Wu, D.; Hanudel, M. R.; Joung, H. A.; Gales, B.; Tseng, D.; Salusky, I. B.; Ozcan, A. Measurement of serum phosphate levels using a mobile sensor. *Analyst* **2020**, *145*, 1841−1848.
(12) Zaman, Z.; Sneyers, L.; Van Orshoven, A.; Blanckaert, N.; Mariën, G. Elimination of paraprotein interference in determination of plasma inorganic phosphate by ammonium molybdate method. *Clin. Chem.* **1995**, *41*, 609−614.
(13) Zhang, Y.; Sheng, S.; Mao, S.; Wu, X.; Li, Z.; Tao, W.; Jenkinson, I. R. Highly sensitive and selective fluorescent detection of phosphate in water environment by a functionalized coordination polymer. *Water Res.* **2019**, *163*, 114883.
(14) Sarwar, M.; Leichner, J.; Naja, G. M.; Li, C.-Z. Smart-phone, paper-based fluorescent sensor for ultra-low inorganic phosphate detection in environmental samples. *Microsyst. Nanoeng.* **2019**, *5*, 56.
(15) Gao, N.; Huang, J.; Wang, L.; Feng, J.; Huang, P.; Wu, F. Ratiometric fluorescence detection of phosphate in human serum with a metal−organic frameworks-based nanocomposite and its immobilized agarose hydrogels. *Appl. Surf. Sci.* **2018**, *459*, 686−692.
(16) Zhao, L.; Xie, S.; Song, X.; Wei, J.; Zhang, Z.; Li, X. Ratiometric fluorescent response of electrospun fibrous strips for real-time sensing of alkaline phosphatase in serum. *Biosens. Bioelectron.* **2017**, *91*, 217−224.
(17) Qin, L.; Wang, X.; Liu, Y.; Wei, H. 2D-metal−organic-framework-nanozyme sensor arrays for probing phosphates and their enzymatic hydrolysis. *Anal. Chem.* **2018**, *90*, 9983−9989.
(18) Zhang, G.; Yu, K.; Zhou, B.; Wang, J.; Zheng, C.; Qu, L.; Chai, H.; Zhang, X. Magnetic zirconium-based Prussian blue analog nanozyme: enhanced peroxidase-mimicking activity and colorimetric sensing of phosphate ion. *Microchim. Acta* **2022**, *189*, 220.
(19) Yan, Z.; Li, Y.; Wei, X.; Li, P.; Jiang, J.; Chen, Y.; Duan, P.; Wang, X.; Deng, P.; Liu, X. Sensitive photoelectrochemical biosensors based on AuNPs/MXenes electrode coupled with light-harvesting UiO-66-NH_2 probes for protein kinase detection. *Biosens. Bioelectron.: X* **2022**, *11*, 100204.
(20) Cavka, J. H.; Jakobsen, S.; Olsbye, U.; Guillou, N.; Lamberti, C.; Bordiga, S.; Lillerud, K. P. A new Zirconium inorganic building brick forming metal organic frameworks with exceptional stability. *J. Am. Chem. Soc.* **2008**, *130*, 13850−13851.
(21) Zou, D.; Liu, D. Understanding the modifications and applications of highly stable porous frameworks via UiO-66. *Mater. Today Chem.* **2019**, *12*, 139−165.
(22) Du, T.; Wang, J.; Zhang, L.; Wang, S.; Yang, C.; Xie, L.; Liu, Z.; Ni, Y.; Xie, X.; Sun, J.; et al. Missing-linker engineering of Eu (III)-doped UiO-MOF for enhanced detection of heavy metal ions. *Chem. Eng. J.* **2022**, *431*, 134050.
(23) Liu, G.; Guo, Y.; Chen, C.; Lu, Y.; Chen, G.; Liu, G.; Han, Y.; Jin, W.; Xu, N. Eliminating lattice defects in metal−organic framework molecular-sieving membranes. *Nat. Mater.* **2023**, *22*, 769−776.
(24) Li, S.; Zhou, Z.; Tie, Z.; Wang, B.; Ye, M.; Du, L.; Cui, R.; Liu, W.; Wan, C.; Liu, Q.; et al. Data-informed discovery of hydrolytic nanozymes. *Nat. Commun.* **2022**, *13*, 827.
(25) Liu, X.; Wang, A.; Wang, C.; Li, J.; Zhang, Z.; Al-Enizi, A. M.; Nafady, A.; Shui, F.; You, Z.; Li, B.; et al. A general large-scale synthesis approach for crystalline porous materials. *Nat. Commun.* **2023**, *14*, 7022.
(26) Kitchenham, B. A.; Rowlands, G. J.; Manston, R.; Dew, S. M. The Blood Composition of Dairy Calves Reared Under Conventional and Rapid-Growth Systems. *Br. Vet. J.* **1975**, *131*, 436−446.
(27) Wen, Z.; Li, H.; Shen, Q.; Tang, X.; Xiong, C.; Li, H.; Pang, J.; Ryan, M. H.; Lambers, H.; Shen, J. Tradeoffs among root morphology, exudation and mycorrhizal symbioses for phosphorus-acquisition strategies of 16 crop species. *New Phytol.* **2019**, *223*, 882−895.
(28) Hruska, K. A.; Mathew, S.; Lund, R.; Qiu, P.; Pratt, R. Hyperphosphatemia of chronic kidney disease. *Kidney Int.* **2008**, *74*, 148−157.
(29) Yuan, S.; Feng, L.; Wang, K.; Pang, J.; Bosch, M.; Lollar, C.; Sun, Y.; Qin, J.; Yang, X.; Zhang, P.; et al. Stable Metal−Organic Frameworks: Design, Synthesis, and Applications. *Adv. Mater.* **2018**, *30*, 1704303.

https://doi.org/10.1021/acsanm.4c03379
ACS Appl. Nano Mater. 2024, 7, 19466−19472